Icarus 218 (2012) 975–988

Contents lists available at SciVerse ScienceDirect

Icarus

journal homepage: www.elsevier.com/locate/icarus

Radiative transfer analyses of Titan's tropical atmosphere

Caitlin A. Griffith [a,*], Lyn Doose [a], Martin G. Tomasko [a], Paulo F. Penteado [b], Charles See [a]

[a] Department of Planetary Sciences, The University of Arizona, Tucson, AZ 85721, USA
[b] Instituto de Astronomia, Geofísica e Ciências Atmosféricas, Universidade de São Paulo, Brazil

ARTICLE INFO

Article history:
Received 27 May 2011
Revised 10 November 2011
Accepted 25 November 2011
Available online 13 December 2011

Keywords:
Titan
Satellites, Atmospheres
Radiative transfer
Infrared observations
Spectroscopy

ABSTRACT

Titan's optical and near-IR spectra result primarily from the scattering of sunlight by haze and its absorption by methane. With a column abundance of 92 km amagat (11 times that of Earth), Titan's atmosphere is optically thick and only ~10% of the incident solar radiation reaches the surface, compared to 57% on Earth. Such a formidable atmosphere obstructs investigations of the moon's lower troposphere and surface, which are highly sensitive to the radiative transfer treatment of methane absorption and haze scattering. The absorption and scattering characteristics of Titan's atmosphere have been constrained by the Huygens Probe Descent Imager/Spectral Radiometer (DISR) experiment for conditions at the probe landing site (Tomasko, M.G., Bézard, B., Doose, L., Engel, S., Karkoschka, E. [2008a]. Planet. Space Sci. 56, 624–247; Tomasko, M.G. et al. [2008b]. Planet. Space Sci. 56, 669–707). Cassini's Visual and Infrared Mapping Spectrometer (VIMS) data indicate that the rest of the atmosphere (except for the polar regions) can be understood with small perturbations in the high haze structure determined at the landing site (Penteado, P.F., Griffith, C.A., Tomasko, M.G., Engel, S., See, C., Doose, L., Baines, K.H., Brown, R.H., Buratti, B.J., Clark, R., Nicholson, P., Sotin, C. [2010]. Icarus 206, 352–365). However the *in situ* measurements were analyzed with a doubling and adding radiative transfer calculation that differs considerably from the discrete ordinates codes used to interpret remote data from Cassini and ground-based measurements. In addition, the calibration of the VIMS data with respect to the DISR data has not yet been tested. Here, VIMS data of the probe landing site are analyzed with the DISR radiative transfer method and the faster discrete ordinates radiative transfer calculation; both models are consistent (to within 0.3%) and reproduce the scattering and absorption characteristics derived from *in situ* measurements. Constraints on the atmospheric opacity at wavelengths outside those measured by DISR, that is from 1.6 to 5.0 μm, are derived using clouds as diffuse reflectors in order to derive Titan's surface albedo to within a few percent error and cloud altitudes to within 5 km error. VIMS spectra of Titan at 2.6–3.2 μm indicate not only spectral features due to CH_4 and CH_3D (Rannou, P., Cours, T., Le Mouélic, S., Rodriguez, S., Sotin, C., Drossart, P., Brown, R. [2010]. Icarus 208, 850–867), but also a fairly uniform absorption of unknown source, equivalent to the effects of a darkening of the haze to a single scattering albedo of 0.63 ± 0.05. Titan's 4.8 μm spectrum point to a haze optical depth of 0.2 at that wavelength. Cloud spectra at 2 μm indicate that the far wings of the Voigt profile extend 460 cm^{-1} from methane line centers. This paper releases the doubling and adding radiative transfer code developed by the DISR team, so that future studies of Titan's atmosphere and surface are consistent with the findings by the Huygens Probe. We derive the surface albedo at eight spectral regions of the 8 × 12 km^2 area surrounding the Huygens landing site. Within the 0.4–1.6 μm spectral region our surface albedos match DISR measurements, indicating that DISR and VIMS measurements are consistently calibrated. These values together with albedos at longer 1.9–5.0 μm wavelengths, not sampled by DISR, resemble a dark version of the spectrum of Ganymede's icy leading hemisphere. The eight surface albedos of the landing site are consistent with, but not deterministic of, exposed water ice with dark impurities.

1. Introduction

Prior to the Cassini/Huygens mission, studies of Titan's atmospheric composition, cloud characteristics, surface, and energy partitioning relied on an opacity structure due to methane and haze that was incompletely constrained in the lower atmosphere. Before Huygens descended into Titan's atmosphere in January 2005, the methane abundance and haze scattering profiles were estimated from remote ground-based, HST, and Voyager measurements of Titan's I/F or occulted transmission, coupled with thermodynamic arguments based on the temperature profiles measured

* Corresponding author.
E-mail address: griffith@lpl.arizona.edu (C.A. Griffith).

0019-1035/$ - see front matter © 2011 Elsevier Inc. All rights reserved.
doi:10.1016/j.icarus.2011.11.034

Table 1
Huygens DISR VIS Cassini VIMS measurements.

	VIMS VIS	VIMS IR	DISR VIS	DISR IR
Spectral range	0.35–1.07	0.85–5.1	0.48–0.96	0.85–1.6
Spectral resolution (FWHM)	0.007 μm	0.014 μm	0.0058 μm	0.017 μm
Angular resolution	0.5×0.5 mrad^2	0.5×0.25 mrad^2	4°×4°	9°×360°
Highest spatial resolution	0.5×0.5 km^2	0.5×0.25 km^2	4×4 cm^2	4×4 cm^2
Spatial resolution of this data	–	8.5×20.3 km^2	0.5×0.5 km^2	0.5×0.5 km^2
RT program	Discrete ordinates	Discrete ordinates	Doubling and adding	Doubling and adding
Number of spectra	11,633,066	11,633,066	6234	9146
Terrain coverage	Pole to pole	Pole to pole	60×60 km^2	60×60 km^2

by Voyager (Lindal et al., 1983; Rages and Pollack, 1983; Flasar et al., 1981; Lellouch et al., 1989; Griffith et al., 1991; Rannou et al., 2003; McKay et al., 2001). The saturation mixing ratio of methane at the tropopause (0.017) provided an upper limit to the stratospheric methane abundance. However, below 50 km, the methane abundance and surface humidity remained largely unconstrained, with values ranging from 25% to 200% humidity (Courtin et al., 1995; McKay et al., 1997; Samuelson et al., 1997). Remote measurements of the tropospheric methane profile were difficult, because most of the methane lines that defined Titan's spectrum were saturated and thus largely insensitive to the methane abundance (Griffith et al., 1991). The only non-saturated lines are weak ones whose intensities were unknown until recently (Penteado and Griffith, 2010; de Bergh et al., 2012).

Prior to the Cassini/Huygens mission, Voyager and ground-based observations led to good estimates of the haze production rate. In addition it was realized that Titan's aerosols have a fractal shape, and the atmosphere's extinction profile changes at ~100 km and also below 30 km (West and Smith, 1991; Israel et al., 1991; Cabane et al., 1992; Tomasko et al., 1997; Young et al., 2002; Rannou et al., 2003). Yet information regarding Titan's haze below 100 km was hindered by the opacity of the overlying atmosphere and the need for simultaneously constraining the phase function, single scattering albedo (SSA) and optical depth. Thus, the moon's backscattered radiation as measured from Earth could be interpreted with a range of solutions (Young et al., 2002; Tomasko et al., 1997; Rannou et al., 2003).

The Huygens Probe provided the first *in situ* measurements of the haze and composition in Titan's lower atmosphere. As the probe descended through Titan's atmosphere, the onboard spectrometers in DISR, measured the diffuse and direct radiation at a range of scattering angles, at 0.4–1.6 μm, and at altitudes that extended from the surface up to nearly 150 km altitude (Tomasko et al., 2005). The upward and downward looking spectra obtained by DISR during descent were used to determine the scattering properties of both the surface and atmosphere. The intensity of the direct beam, measured while looking upward and towards the Sun constrained the optical depth and single scattering albedo with altitude (Tomasko et al., 2005). The phase function of the atmospheric aerosols was derived from photometry of the solar aureole and its agreement with the scattering properties of fractal aggregate particles. The result is a measurement of the single scattering albedo, scattering phase function and haze optical depth as a function of wavelength and altitude (Tomasko et al., 2008b). This information indicates the particles' shape, size, indices of refraction, and haze density as a function of altitude at the landing site at −10° latitude, 192° west longitude at the time of the landing. In addition, DISR's measurement of methane absorption combined with the GCMS determination of the methane vertical abundance profile constrained the methane absorption characteristics (Tomasko et al., 2008a; Niemann et al., 2005, 2010). The downward looking spectrometers, in addition to the on-board lamp, constrained the surface albedos.

Huygens DISR measurements significantly updated our understanding of the haze characteristics. For example, the optical depth at 0.5 μm was determined to be $\tau = 4.5$ in the most comprehensive pre-Cassini/Huygens analysis (Rannou et al., 2003), and $\tau = 7$ by Huygens DISR (Tomasko et al., 2008b). Many prior models required a depletion of haze below ~80 km altitude (Young et al., 2002; Tomasko et al., 1997; Rannou et al., 2003). These models have been replaced by the Huygens-derived haze structure, which consists of three layers: one above 80 km, another between 30 km and 80 km, and a final layer below 30 km (Tomasko et al., 2008b). The appearance of a haze depletion below 80 km is now understood to be caused by changes in the haze properties, i.e. the phase function, single scattering albedo, and extinction (Tomasko et al., 2008b), that largely result from HCN and CH_4 condensation (Lavvas et al., 2011). The methane absorption characteristics have been updated, because for example the most rigorous derivations prior to the Huygens measurements overestimated the absorption by a factor of 3 at some wavelengths and underestimated values by a factor of 10 at other wavelengths (Tomasko et al., 2008a).

The analysis of the *in situ* DISR measurements that led to the derivation of Titan's haze and methane properties was conducted with the doubling and adding radiative transfer code described in Appendix A. The interpretation of remote observations (e.g. ground-based and Cassini VIMS data) generally use the publicly available discrete ordinates code called DISORT (Stamnes et al., 1988), because it is ~10 times faster than doubling and adding calculations, and thus better suited for the analysis of tens of thousands of images formed by thousands of spectra (Table 1). The question then arises as to whether these two radiative transfer analyses are indeed equivalent, given certain assumptions in each radiative transfer technique, and whether the DISR and VIMS observations are consistently calibrated to render similar results. In addition, current published radiative transfer analyses of Titan's optical and near-IR spectra range in complexity. For example, some models use 2 stream and others 32 stream radiative transfer calculations, which yield vastly different treatments of the scattering properties of Titan's atmosphere. As a result, conflicting interpretations of measured spectra arise that are not a result of a poorly understood atmosphere, but, rather, from overly simplified treatments of the scattering and absorption properties, which render some models inconsistent with prior measurements. Huygens measurements provide the needed reference point characterization of the atmosphere from which models can be tested.

This paper focuses on the analysis of Cassini VIMS data of the landing site, particularly within the eight spectral regions between 0.8 and 5.1 μm often called "windows", that probe the lower atmosphere and surface; these are centered at 0.93, 1.08, 1.28, 1.58, 2.02, 2.76, and 5.00 μm. Within the spectral region sampled by DISR (0.4–1.6 μm), we analyze VIMS data with the DISR doubling and adding code, as well the discrete ordinates code, to assess both the consistency of the VIMS and DISR data, and to derive a discrete ordinates model that reproduces the results of the DISR doubling and adding code. We discuss the structure and usage of the DISR

doubling and adding code, and make the code available at a public website (Appendix A). In addition, benchmark tests and calculated spectra are presented, which can be used to evaluate other models for their consistency with Huygens measurements (Appendix B). At longer wavelengths not sampled by *in situ* measurements, we investigate the opacity structure of the atmosphere, using VIMS data and available information on methane absorption and Titan's haze, in order to derive constraints on the atmosphere's optical depth and scattering characteristics. The paper closes with a derivation and discussion of the surface albedo of the landing site area at the 8 spectral windows.

2. Model of Titan's atmosphere

Constraints on the scattering and absorption properties of Titan's atmosphere as determined from Huygens DISR measurements are summarized in Tomasko et al. (2008b) and Tomasko et al. (2008a). At the wavelengths directly measured by DISR (0.4–1.6 μm), we adopt their derived haze single scattering albedo, phase function and optical depth. Rayleigh scattering of N_2 is included. In addition, at these wavelengths, we use methane coefficients derived by DISR measurements (Tomasko et al., 2008a), but with an adjustment. These coefficients were determined relative to the absorption at 1.28 μm, which was found to be very low and thus assumed to be zero. However, recent laboratory data (the first that reproduce Titan's conditions) indicate, to the contrary, an absorption coefficient of 0.02 (km amagat)$^{-1}$ at this wavelength (de Bergh et al., 2012). Therefore, 0.02 (km amagat)$^{-1}$ was added to all of the DISR absorption coefficients (Tomasko et al., 2008a). The resultant methane absorption coefficients produce I/F values intermediate between those of Tomasko et al. (2008a) and a new study by Karkoschka and Tomasko (2010). In addition, we assume that the haze phase function derived by DISR for levels above 80 km, which has no backscattering peak, applies to the entire atmosphere. This was assumed because although the visible spectrometer was able to discern backscattering peaks, the DISR IR spectrometer integrated for more than one rotation of the probe, so there is no evidence for or against a backward peak from the measurements longward of 1 μm. In addition, estimates of the phase function from fractal models predict no backward peaks longward of 1 μm wavelength.

At wavelengths longer than 1.6 μm, we calculate absorption coefficients using line-by-line analyses of the CH_4, CH_3D and CO HITRAN line parameters (Rothman et al., 2009). The pressure-broadened lines have contributions that are expected to be overestimated by the Voigt profile in the far wings in such a way that is not well quantified yet. We parametrize this effect by truncating the lines at a "cutoff" distance from the line center, which is varied to assess the effects of the uncertainty in the line shapes. Where indicated these calculations are compared to the absorption coefficients of Karkoschka and Tomasko (2010). As discussed below, neither of these absorption parameters entirely explains the observed spectral features within the 2 μm window. At 4.6–5.0 μm we include CO absorption, also from the HITRAN data base; however we omit the effects of solar-excited fluorescence, which causes us to underestimate the flux at ~4.75 μm (Lellouch et al., 2003). However, studies of Titan's troposphere and surface (which we focus on here) require an analysis at 4.9–5.1 μm, outside the CO band, and are unaffected by the neglect of fluorescence.

The haze single scattering albedo remains unconstrained outside of the wavelengths covered by Huygens/DISR. We do not attempt to derive the particle single scattering albedo at these longer wavelengths, because VIMS data measure only the backscattered sunlight, which is also affected by the likely variable surface albedo probed within the footprint of the pixel, as well as the scattering phase function. Methane ice spectral features are also difficult to discern, because the clouds are viewed through a methane rich atmosphere. Therefore we assume the optical properties of spherical ice and liquid methane drops (above and below 15 km respectively) for Titan's clouds. For the haze we adopt the optical properties of tholins, the laboratory analogs to Titan's haze (Khare et al., 1984), for wavelengths outside those measured by Huygens. In addition, HCN polymers (Khare et al., 1994) are considered to explore the effects of a multi-compositional haze population. We use the haze optical depth derived by DISR measurements for 0.4–1.6 μm wavelengths, and extrapolated to much longer wavelengths (~5 μm), where the effects of a 30% uncertainty are considered. The surface albedo is assumed to be Lambertian and of constant albedo across the windows.

3. Radiative transfer approximations

The radiative transfer equation in a non-isotropic and non-uniform scattering atmosphere defines the attenuation of the intensity, I_λ at each wavelength, λ:

$$\frac{dI_\lambda}{d\tau_\lambda} = -I_\lambda + S_\lambda, \tag{1}$$

which depends not only on the incident radiation (first term on right-hand side), but also on the source function, S_λ (second term). For Titan's lower atmosphere (not considering fluorescence), the near-IR source function represents simply the scattering of light into the beam:

$$S_\lambda = \frac{\omega_\lambda}{4\pi}\int_{4\pi} d\Omega' p(\theta',\phi';\theta,\phi) I_\nu(\theta',\phi'), \tag{2}$$

and depends on the phase function, $p(\theta',\phi';\theta,\phi)$, which quantifies the probability that light, in the direction of polar angle, θ', and azimuthal angle, ϕ' is scattered in a particular direction (θ,ϕ). This source function also depends on the single scattering albedo, ω_λ, the probability that an extinction event causes scattering. The integral above (Eq. (2)) can be analytically solved only for a single scattering event, in which case:

$$S_\lambda = \frac{\omega_\lambda}{4\pi} p(\theta',\phi';\theta,\phi) F^s e^{-\tau/\mu'} \tag{3}$$

where F^s is the irradiance, τ is the total optical depth of the medium, and μ' is $\cos(\theta')$. Otherwise the solution must be approximated for a non-isotropic and non-uniform atmosphere.

This study concerns only low phase angle spectra of small areas of Titan's surface, such that the atmosphere can be approximated as a stack of parallel slabs, wherein the atmosphere is estimated to be uniform (e.g. constant composition, pressure and temperature). The doubling and adding technique further divides these slabs into thin enough layers such that one can assume at most one scattering event ($\Delta\tau \sim 10^{-8}$). The equation for radiative transfer can then be solved analytically (Eqs. (1) and (3)). The resulting reflection and transmission functions are used to solve for a layer twice the thickness, and the resulting *doubling method* is used to derive the scattering and absorption characteristics for each uniform thick slab. The solutions for the slabs are then combined, or *added*, to determine the scattering behavior for the entire non-uniform atmosphere.

While the discrete ordinates method also assumes a plane-parallel atmosphere, it is an entirely different approach. Here the integral in the source function is approximated by a discrete sum over the polar angles, θ and θ', sampled by $N/2$ angles (or ordinates) in the downward direction, and $N/2$ angles in the upward direction, where N is the number of streams. The phase function is often approximated by a series of N Legendre polynomials, for which the polar and azimuthal coordinates are separable. Then the

azimuthal dependence on the phase function can be estimated using a Fourier series. This method, considering an azimuthally independent example, replaces the radiative transfer equation (Eqs. (1) and (2)) with N coupled equations corresponding to the intensities (Eq. (1)) in all N directions.

Detailed descriptions of the doubling and adding and the discrete ordinates analyses are presented in Appendix A, where we show that the discrete ordinates calculation, despite its different treatment of the phase functions, yields spectra that differ from those calculated by the doubling and adding code to within 0.3%. Appendix A also presents the updated phase functions that enable this agreement between the two models. Appendix B indicates the website of the Huygens DISR doubling and adding code and supplies benchmark spectra of our calculations, which can be used to test codes for their consistency with the DISR analysis of the *in situ* measurements of Titan's atmosphere.

4. Cassini and Huygens spectra of the landing site

During the TB Titan flyby on 13 December 2004, VIMS targeted the probe landing site, recording data close enough in time to the Huygens landing on 14 January 2005, that the atmosphere will not have changed as a result of the seasonal variations. Three spectra were selected from the TB-V1481624349 image cube, which cover the landing site region (Fig. 1), at a low phase angle (18.63°), incident angle (36.72°), and scattering angle (35.13°). The delta azimuthal angle of 148° indicates a backscattering geometry. The footprint of each pixel extends an area of 8×21 km^2, thereby covering both the dark plains and the surrounding hills (Fig. 1). These data are analyzed to constrain the surface albedo of the landing site at wavelengths not sampled by Huygens, and to evaluate the consistency of the radiative transfer calculations as well as that of the Cassini VIMS and Huygens DISR spectra where these two measurements overlap.

The Huygens DISR instrument measured Titan's surface albedo both with and without illumination by the on-board lamp. The lampless measurements of the surface reflectivity were determined during descent using the downward looking spectrometers (Schröder and Keller, 2009). These measurements provide a good estimate of the albedos sampled remotely by Cassini, because they include light scattered at a range of phase angles (10–55°), more typical of the diffusely scattered light observed by Cassini. Additionally favorable, at these angles, Titan's surface displayed a largely isotropic scattering behavior (Schröder and Keller, 2009). In contrast, the lamp-illuminated surface consisted purely of backscattered radiation, which indicated a non-isotropic peak (Schröder and Keller, 2009).

We considered two sets of DISR observations of the surface albedos: those recorded during the last 0.07–1 km of Huygens' descent, when the lamp reflection was not visible, and those recorded at higher altitudes, which sample the larger surrounding region. The close-up observations targeted a region within 1 km of the landing site (Schröder and Keller, 2009); these albedos pertain entirely to the dark floodplains. The latter observations measured mostly subtle differences between the surface reflectivity of the landing site and that of the brighter highlands (Fig. 2). The uplands were found to be 12–18%, 12–18%, 18–21%, 22–25% and 63–71% brighter than the landing site at 0.083, 0.93, 1.07, 1.28, and 1.59 μm, respectively (Keller et al., 2008).

5. Analysis of VIMS observations

The three VIMS spectra that cover the terrain measured by the Huygens Probe (Fig. 1) exhibit subtle I/F variations (Fig. 3), consistent with the lack of large surface albedo variations as determined by DISR (Keller et al., 2008). To derive the surface albedo, we assume the DISR-derived haze, the adjusted methane absorption coefficients, and, for the discrete ordinates model, the haze phase function Legendre coefficients detailed in Appendix A. We also

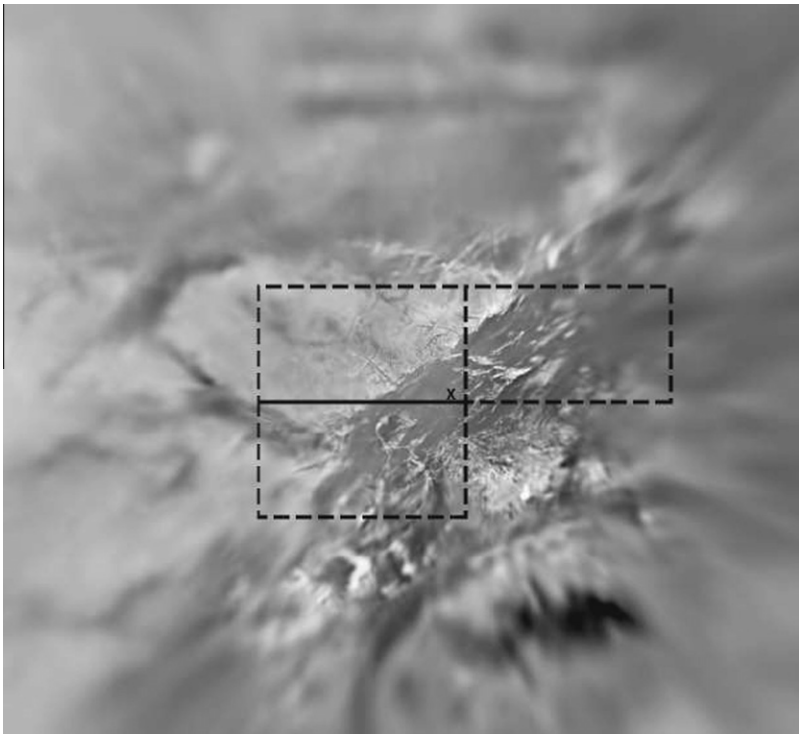

Fig. 1. Huygens DISR image of the landing site (marked with an "×") from images recorded during descent. The footprint of pixels [11,2], [11,3], and [10,2] of the VIMS V1481624349 cube, shown as the left, right and bottom boxes, respectively.

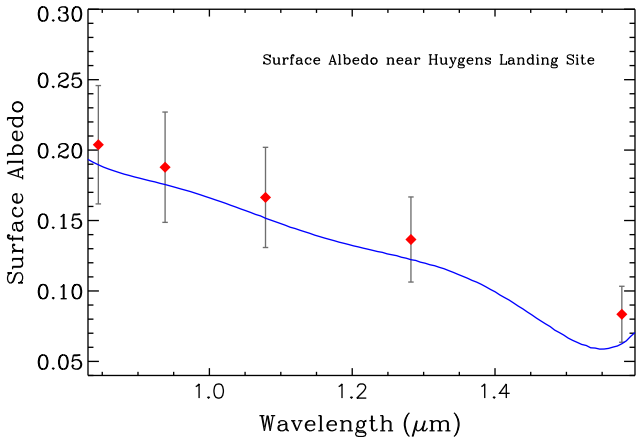

Fig. 2. Titan's surface albedo measured by the DISR downward looking spectrometers during the last kilometer of descent (solid line). Adjusted surface albedos (diamonds), at "window" wavelengths, for a surface composed of half landing site terrain and half brighter "uplands", assuming the contrasts of Keller et al. (2008). Uncertainties (shown by error bars) result from the method in which the atmospheric effects were estimated (Keller et al., 2008).

assume a Lambertian surface, consistent with Huygens descent measurements (Schröder and Keller, 2009), and explore the effects of the brighter highlands in the field of view by considering a surface half composed of the "brighter terrain" (Figs. 2 and 3).

Our study indicates that VIMS data are consistent with DISR measurements, and the DISR radiative transfer analysis agrees with the discrete ordinates radiative transfer analysis. With the derived Legendre coefficients (Appendix A), the discrete ordinates calculation and the doubling and adding DISR code derive the same outgoing intensity, to within 0.3% for the same surface albedo and atmospheric parameters (Appendix A). The resultant surface albedos that match the VIMS spectra are 0.21 ± 0.04, 0.18 ± 0.04, 0.17 ± 0.02, 0.14 ± 0.02, and 0.08 ± 0.02 within the 0.82, 0.93, 1.08, 1.28 and 1.58 μm window respectively; these agree with values obtained by DISR measurements (Fig. 2).

Cassini VIMS spectra also cover wavelengths at 1.6–5 μm, which were not sampled by the Huygens Probe. While the methane opacity is not constrained by *in situ* measurements, the methane abundance profile is known at the landing site. In addition, the haze optical depth at the DISR wavelengths are used to estimate through extrapolation the optical depth at the longer wavelengths measured by VIMS. Here we investigate the opacity structure of Titan's atmosphere particularly at spectral regions surrounding the atmospheric windows, i.e. at 2 μm, 2.8 μm and 5 μm, by considering available data on the gas absorption and scattering by likely particulates. We also analyze spectra of clouds, which act as diffuse reflectors, thereby allowing us to somewhat constrain the curve of growth of atmospheric absorption.

5.1. The 1.99–2.18 μm window

Titan's 2 μm window is obscured not only by methane but also by pressure-induced H_2–H_2, H_2–N_2 and N_2–CH_4 absorption (Griffith et al., 1991). We assume a hydrogen abundance of 0.1% (Niemann et al., 2010), and adopt the absorption coefficients of McKellar (1989). Both the HITRAN methane parameters and the absorption coefficients derived by Karkoschka and Tomasko (2010) are considered. Also included are the optical constants of tholins, which provide a good interpretation to the spectrum at 2.2–2.3 μm where methane lines are saturated and the spectrum is therefore insensitive to the detailed methane parameters and the surface.

Titan's gas opacity in the 1.9–2.3 μm region appears to be poorly understood. A calculation of the spectrum with HITRAN methane line parameters depends strongly on the choice in the truncation of the lines at a cutoff distance from the line center, as shown for two examples in Fig. 4. The methane absorption coefficients derived by Karkoschka and Tomasko (2010) do not agree with the line parameters compiled in HITRAN. None of the calculations match the shape or, for the most part, the I/F throughout much of the 1.9–2.18 μm spectral region. The mismatch between the data and calculations are seen for measurements over all terrain types and over cloudy regions, suggesting that while the surface may play a role, the atmosphere is also a culprit.

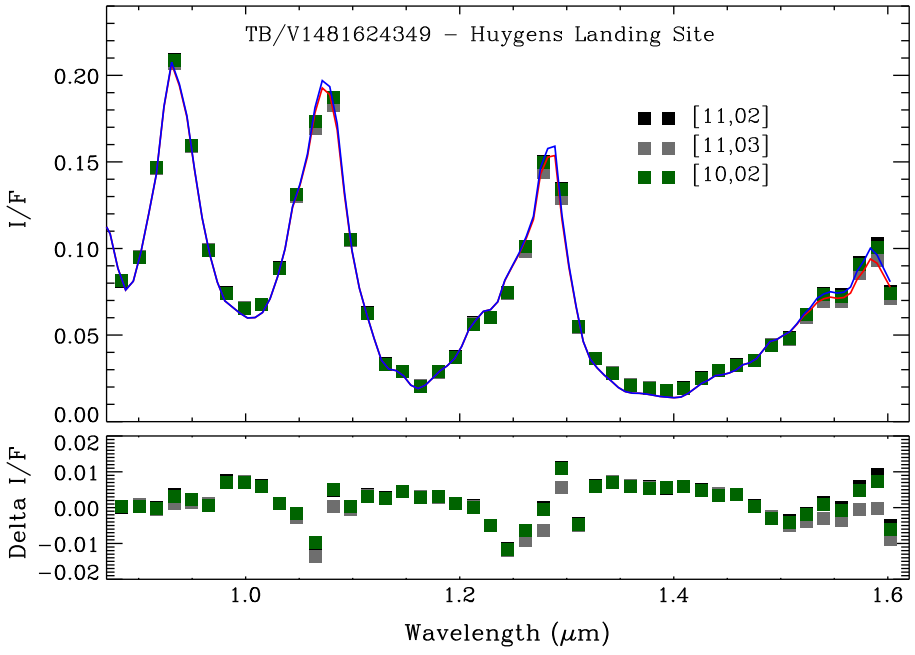

Fig. 3. VIMS Spectra of the probe landing site (cube: V1481624349; pixels: [11,2], [11,3], and [10,2]), shown as squares, are compared to models that assume the landing site surface (red), and half landing site and half uplands surface (blue). Differences between the model (red) and the three observations are shown in the lower panel. The pixel footprints appear in Fig. 1.

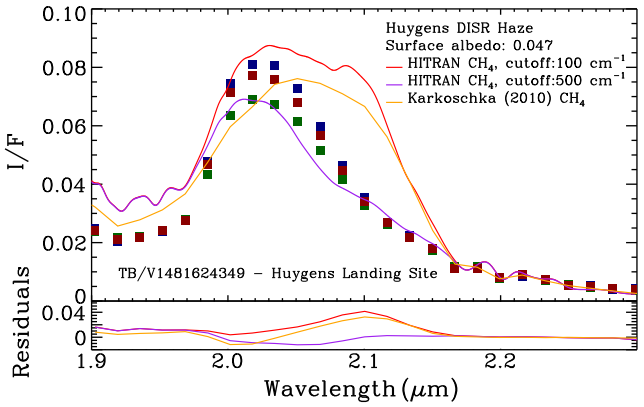

Fig. 4. Spectra from VIMS TB-V1481624349 cube (squares) are compared to models (lines) which all assume the DISR estimated optical depth of Titan's haze and the Huygens Probe methane abundance profile, but which adopt different methane absorption coefficients. Red and purple models were calculated from line parameters, assuming the different indicated cutoff distances from line centers of the wings of the Voigt profiles. The orange model derives from the absorption coefficients of Karkoschka and Tomasko (2010). The surface albedo was assumed constant within the window.

To explore the cause for this mismatch we analyze spectra of low and high clouds, which serve as diffuse reflectors at known altitudes. Titan's methane clouds consist of particles larger than 5 μm, which have a relatively uniform optical depth across the near-infrared wavelengths. Therefore, the scattering characteristics (the effective altitudes and optical depths) of the cloud can be established from the 1.0–1.6 μm measurements, where the atmospheric opacity was determined from DISR measurements. We can then test whether the derived cloud altitude and optical depth also matches the 2.0 μm region, and thereby evaluate the opacity of this window.

We consider one of the lowest and thickest clouds yet identified in VIMS spectra of Titan's tropical atmosphere, that recorded in the V1590646944 spectral image of the T44 Titan flyby. In addition, we consider the higher cloud in the VIMS V1481607233 spectra image of the TB Titan flyby. The independent analysis of the 1.08, 1.28, 1.58, and 2.00 μm window spectra of the V1481607233 cube indicate the presence of a cloud at 31 ± 5 km altitude, with an optical depth of ~0.26, as discussed in more detail in the next section. The study of this cloud indicates that there is no large discrepancy in the 2 μm opacity above 30 km, since the same cloud parameters are derived from all wavelengths.

With respect to the V1590646944 spectral image, the analysis of the 1.08, 1.28, and 1.58 μm window spectra lead independently to a cloud altitude of 16 ± 4 km with an optical depth of ~8 (Griffith et al., 2009). However, the 1.99–2.18 μm spectra indicate a range of solutions, which depend on the cutoff of the far wings of the methane lines. We derive a cloud altitude of less than 5 km for the cutoff of 100 cm^{-1}, and an altitude of 16 ± 6 km for a cutoff of 460 cm^{-1} (Fig. 5). The uncertainties given here represent the variation in the fit of the model spectrum to the observation. A far wing cutoff of ~460 cm^{-1} for the methane lines is thus indicated, as it leads to consistent derivations of cloud altitudes. Yet the methane far wings do not fully explain the opacity structure. The effect of the cloud is underestimated in the model at 2.00–2.05 μm (Fig. 5), indicating that the atmospheric opacity, and thus the surface albedo, are both overestimated in this model.

Because of the evident uncertainties in the opacity of the Titan's atmosphere, we derive the range of surface albedos at 2 μm for the landing site spectra (Fig. 4) that match the center I/F of the window, considering both the HITRAN parameters and Karkoschka and Tomasko (2010) coefficients for methane, and the uncertainty in the far wings shape. The 2 μm surface albedo so determined is 0.047 ± 0.02, where the uncertainty represents the spread in the surface albedos caused by considering the different methane absorption sources detailed above.

5.2. The 2.65–2.90 μm window

Titan's spectrum within the 2.3–3.3 μm region is affected primarily by absorption due to CH_4 and CH_3D, and, perhaps as significantly, by haze. At 2.6–3.2 μm, the moon's spectrum displays features that match those of CH_4 and CH_3D (Coustenis et al., 2006; Rannou et al., 2010). This resemblance is evident in a model that omits the effects of haze absorption (the single scattering albedo of haze is set to 0.98) and includes only absorption due to methane (Fig. 6, top panel). Although the spectral features match, the calculated I/F values are everywhere higher than those observed, even at wavelengths where the atmospheric opacity is too high to probe the surface. The wavelengths sensitive to Titan's surface can be determined by comparing the spectra of bright and dark surface terrains (Fig. 7). We find that the surface is sampled by

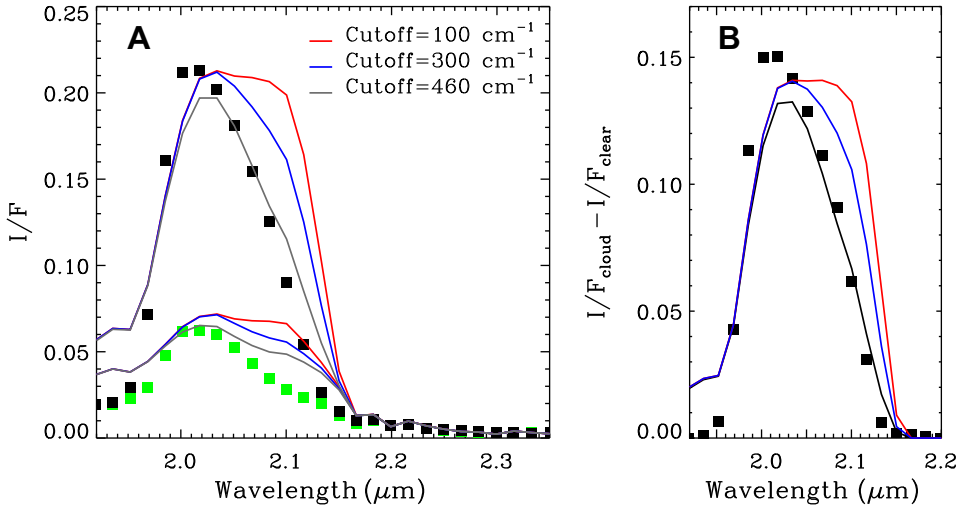

Fig. 5. Three calculations are compared to the V1590646944 spectra of pixels [33,21] and [33,24] of the clear (green squares) and cloudy (black squares) atmosphere, and shown as (A) the I/F values, and (B) the cloud minus clear I/F values. Synthetic spectra were calculated from models that are identical, except in the assumed cutoff distances from the centers of the methane lines. The derived cloud altitude of 16 km (Griffith et al., 2009), and a surface albedo of 0.022 are also adopted.

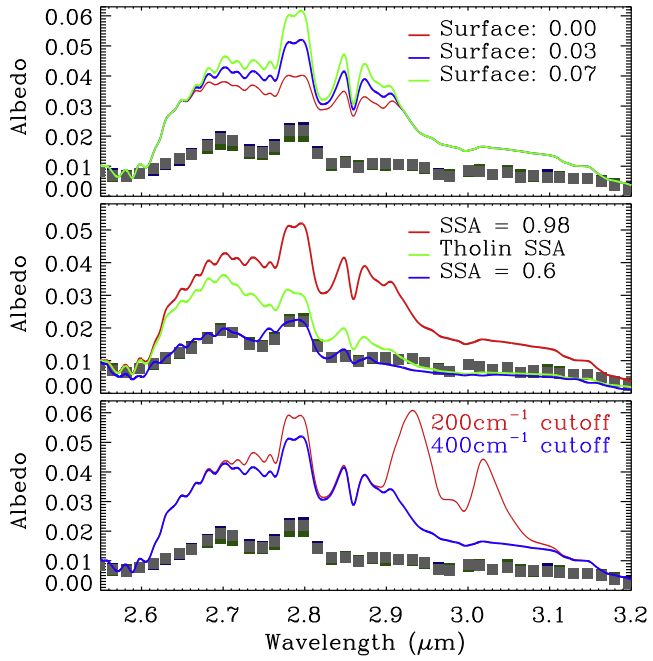

Fig. 6. Calculations (lines) of 3 spectra from VIMS V1481624349 cube (squares) of the same pixels indicated in Fig. 3. Models assume the DISR-derived optical depth of Titan's haze, the Huygens Probe methane abundance profile (Niemann et al., 2005), and HITRAN methane line parameters and partition functions (Rothman et al., 2009). All models assume a CH_4 line wings cutoff of 350 cm^{-1}, and surface albedo of 0.034, and a SSA of 0.98, unless indicated. Top: Models that assume no haze absorption ($SSA_{haze} = 0.98$) and several surface albedos. Middle: Models with different haze SSA. Bottom: Models with different CH_4 line wings cutoffs.

nine VIMS wavelength points between 2.68 and 2.82 μm at a signal above the noise level (Fig. 7). This surface sensitivity agrees with that implied by models at 2.5–2.82 μm, but indicates that model atmospheres are too transparent at 2.82–2.92 μm (Fig. 6, top panel). Also, more absorption is needed throughout the 2.6–3.1 μm region. Therefore, an additional source of atmospheric absorption, which is relatively featureless, is implied by Titan's spectrum.

While HCN and C_2H_2 affect Titan's spectrum outside the window, at 3 μm, none of the known abundant gases, aside from CH_4 and its isotopologues, play a role in opacity structure of the window. The shape of the far wings of the methane lines strongly affects wavelengths longward of the 2.8 μm window (Fig. 6, bottom panel). Yet, the optimal treatment of the far wings is not evident. The simplest method is to truncate the far wings of the profile at a certain "cutoff" distance from the line center. Models that assume a cutoff at 200 cm^{-1} and 400 cm^{-1} are shown in Fig. 6 (bottom panel). Neither fits the data. The former creates a window to Titan's surface at 2.9 μm, which disagrees with the spectral characteristics and transparency of Titan's atmosphere (Fig. 6, bottom panel). The latter provides too much absorption such that the subtle CH_4 features between 2.9 and 3.1 μm are entirely muted. This study suggests that a gentle dampening of the far wings, as indicated by the work of Coustenis et al. (2006), as opposed to a truncation in the line profile, used here, is most realistic. Yet, as the nature of the far wings does not strongly affect the I/F values of the nine wavelengths that define this atmospheric window, we do not explore this uncertainty further.

Since no additional spectral features are indicated at 2.6–2.82 μm, by default we consider alterations to Titan's haze. Nonetheless, it is possible that the missing opacity results from weak methane lines that do not change considerably the overall character of the spectral features. Within this spectral region, laboratory produced analogs of Titan's haze, called "tholins", have single scattering albedos that change dramatically, such that the imaginary index of refraction increases from 10^{-3} to 0.08 at wavelengths between 2.4 and 3.0 μm (Khare et al., 1984), as a result of the N–H stretch vibration. Models that assume the single scattering albedo of tholin particles, match the data only at long wavelengths largely outside the spectral window (Fig. 6, middle panel), and only if the particle size is at least 3 μm, assuming Mie scattering (Fig. 8). The spectral regions outside the window to either side, that is the wavelength regions 2.64 and 2.82 μm, that do not probe the surface, indicate instead the same haze single scattering albedo, 0.63 ± 0.05. A simple solution is suggested by the data: a haze single scattering albedo of 0.63 ± 0.05 between 2.64 and 2.82 μm (Fig. 8). This assumption provides a good fit to the data and indicates a surface albedo of 0.038 ± 0.015 (Fig. 6, middle panel). Here the uncertainty refers to the range of single scattering albedos that match spectral regions unaffected by the surface (Fig. 8). Errors due to noise are, by comparison, insignificant.

Our adjustment of the opacity of Titan's atmosphere in the 2.6–2.83 μm region involves extrapolating a fit to spectral regions that do not sample the surface to spectral regions that do sample the lower atmosphere and surface (the window). We therefore test the validity of our approximation to Titan's opacity by comparing spectra of a cloud to those of nearby clear regions. The VIMS observation V1481607233, recorded during the TB flyby, reveals a relatively thick discrete cloud at 40°N latitude, at low phase, incident

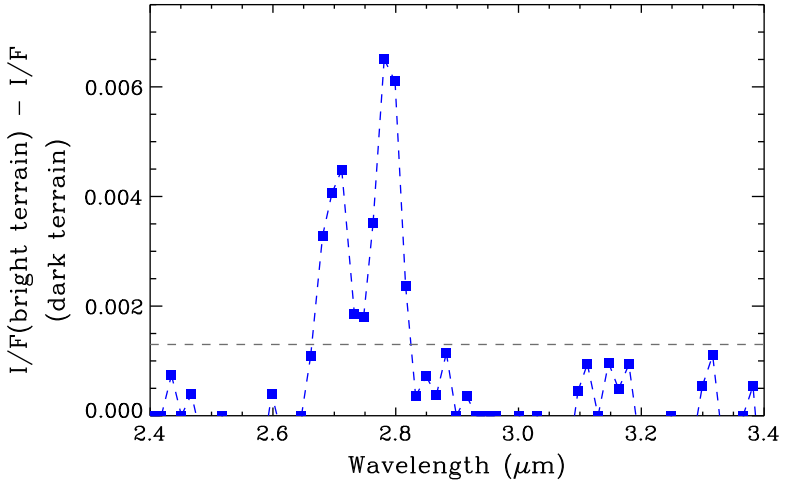

Fig. 7. The difference between the spectra of bright surface and dark surface terrain from the VIMS TB-V1481624349 cube at similar lighting conditions to the landing site data considered here. The spectra are sensitive to the surface above the noise level, shown by the gray line, within the 2.68–2.82 μm wavelength range.

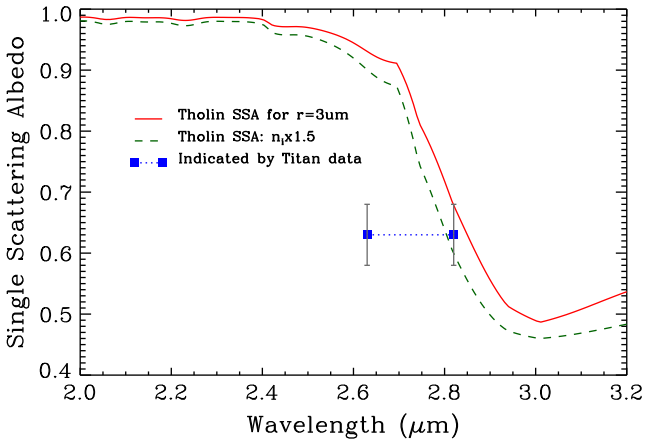

Fig. 8. The single scattering albedos of 3 μm radii tholin particles are compared to values that fit Titan VIMS spectra. They are also compared to the single scattering albedos derived assuming tholin imaginary indices of refraction times 1.5, which is indicated by prior observations of Titan's haze (McKay et al., 1989).

and emission angles of 15.8°, 22°, and 30° respectively. An analysis of the 1–1.6 μm spectra of the cloud-free spectra reveals that the DISR haze model provides a good interpretation of the data for surface albedos of 0.2, 0.17, and 0.13 at 1.08, 1.28 and 1.58 μm, respectively. Keeping the surface albedos fixed, we determine the range of cloud heights and optical depths that match the nearby cloudy spectrum. Clouds enhance Titan's I/F at the spectral regions where sunlight penetrates down to the cloud level. The range of wavelengths affected by the cloud indicates the cloud's height, such that the higher the cloud the larger the range. The cloud's optical depth affects the level of the enhancement (Fig. 9A). We find that the cloud resides at an altitude of 32 ± 5 km, and has an optical depth of 0.26 ± 0.03 (Fig. 9B). The effects of this cloud are more salient at 2.8 μm where its optical depth is similar to that, ~0.65, of Titan's haze.

Titan's 2.8 μm spectra were analyzed assuming the Huygens methane profile, HITRAN compiled methane parameters, and the haze optical depth and phase functions predicted by DISR measurements, basically the same parameters used to study the Huygens landing site data. Following our analysis of the landing site

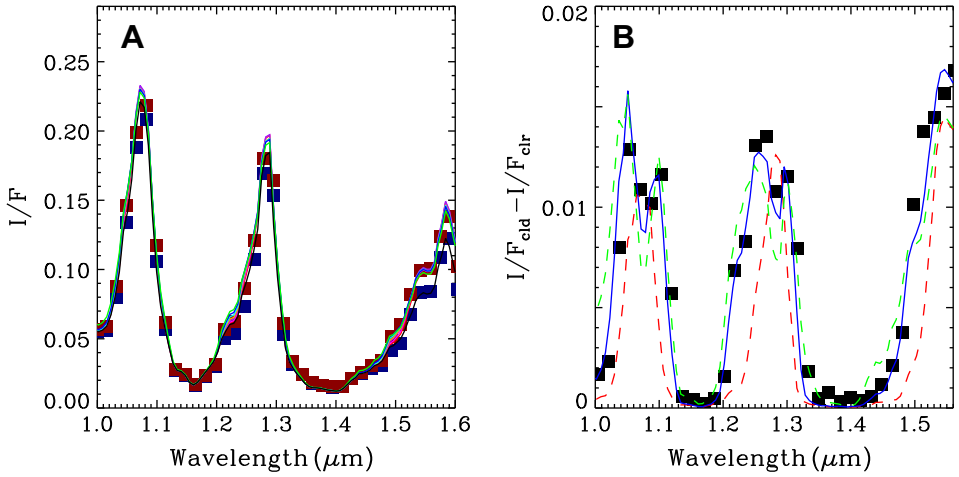

Fig. 9. (A) Spectra of a cloudy (red squares) and clear (blue squares) regions measured in pixels [01,19] and [03,19], respectively, of VIMS cube V1481607233. Lines represent model spectra of clouds at three different altitudes, with an optical depth of 0.26. (B) The difference of measured cloudy and clear atmosphere spectra (black squares) are compared to the difference of calculated cloudy and clear atmosphere spectra for clouds at 11 km (dashed red), 35 km (solid blue) and 50 km (dashed green).

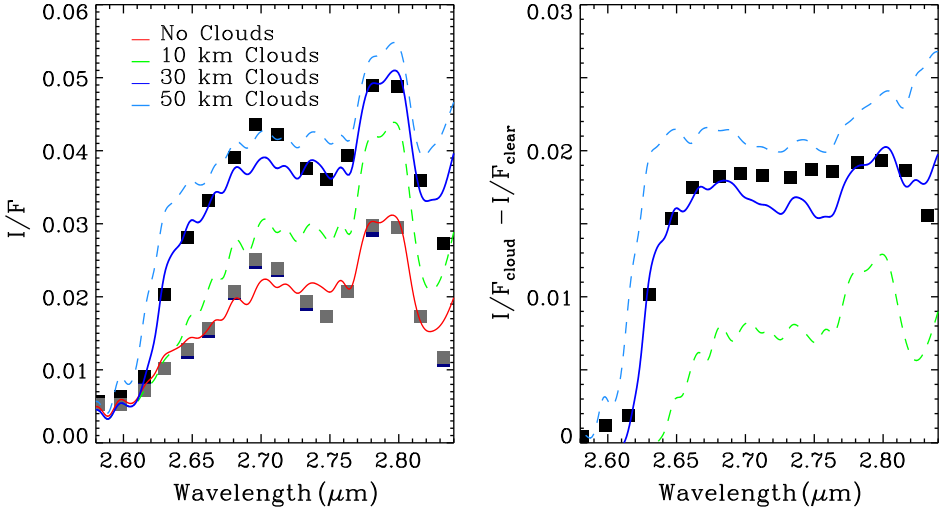

Fig. 10. Left: spectra of cloudy (black squares) and clear (gray squares) regions measured in pixels [01,19] and [03,19], respectively, of VIMS cube V1481607233. Lines represent model spectra of a clear sky (red) and clouds at altitudes of 10 km (dashed green), 30 km (solid blue) and 50 km (dashed light blue), of optical depth 0.26 (blue and green). Right: the difference between calculated cloudy to clear atmosphere spectra for clouds at 10 km (green dashed), 30 km (solid blue) and 50 km (light blue dashed) are compared to that observed.

spectra, the single scattering albedo for the haze was set to 0.6. With these assumptions, the models fit spectra of the clear atmosphere well, and indicate a surface albedo of 0.07 ± 0.005, where the error is the 3σ value due to noise, as determined from both repeated measurements and variations within each spectrum. Models of the cloudy spectrum indicate a cloud optical depth of 0.26 ± 0.05, and a cloud altitude of at 31 ± 4 km altitude (Fig. 10), in agreement with Titan's 1–1.6 μm spectrum. This consistency indicates that although the source of opacity is unknown, the altered haze SSA (to 0.6) provides a good estimate of the opacity structure of Titan's lower atmosphere between 2.68 and 2.82 μm. The detailed definition of the observed features is not a perfect match, which suggests that the detailed wavelength dependence of the extra absorption needs refinement.

5.3. The 4.8–5.1 μm window

The edge of the CO 0–1 fundamental band, where gas absorption becomes insignificant, defines Titan's 5.0 μm window. Here atmospheric particles and the surface albedo establishes Titan's I/F. As the single scattering albedo is unknown, we consider several possible candidates: tholins, methane, ethane, and polyHCN. The indices of refraction of tholins and polyHCN (Khare et al., 1984, 1994) indicate single scattering albedos of 3 μm spherical particles of ~0.95; for methane particles, even as large as 40 μm, similarly high single scattering albedo values are indicated. We therefore adopt a single scattering albedo of 0.95 for the particulates. In addition, we assume an optical depth of 0.3 at 5 μm, and consider the effects of an uncertainty of 30%, since this value was extrapolated from DISR measurements at much lower wavelengths. Spectra at 4.8 μm, which are not strongly affected by fluorescence (Lellouch et al., 2003) indicate an optical depth of 0.2. With these assumptions we derive a surface albedo of 0.03 ± 0.015.

6. Discussion

Our analysis indicates that the Cassini VIMS spectra of the Huygens landing site agree with DISR measurements made during descent, despite the different altitudes, spatial resolution, and spectral resolution of the measurements recorded from these instruments. Because the variations of I/F of the tropical atmosphere between latitudes of 20°S and 20° N are slight, here current models of Cassini VIMS observations can constrain the surface albedo to within 0.05–0.02, depending on the wavelength, and cloud altitudes to within roughly 5 km. The opacity structure at Titan's poles differs from that of the tropical atmosphere, because the particulate population and potentially the methane profile differ from those at the tropics. The derivations of surface albedos and the characteristics of low clouds at the poles is less certain and await extensive spherical radiative transfer derivations of the polar scattering and absorption properties.

We find that Cassini VIMS spectra of the Huygens landing site indicate surface albedos that are consistent with the *in situ* measurements. At the longer wavelengths not sampled by the Huygens Probe, the surface albedo can be estimated from the Huygens constraints on the haze and the methane abundance. At 2 μm, although the opacity structure is poorly constrained (Fig. 4), spectra of clouds provide an indication of the far wings shape of the methane lines, which control the I/F values that define the shape of Titan's spectrum at the 2 μm window. The range in the available absorption coefficients cause a variation of ~0.02 in the derived 2 μm surface albedo. At 2.8 μm, CH_4 and CH_3D match the gross features in Titan's spectrum, yet more opacity is indicated than provided by the available absorption coefficients of methane or by the single scattering albedos of laboratory analogs of Titan's haze. If the haze SSA between 2.64 and 2.82 μm is set to 0.6, the resultant models match the measured spectra both in and out of the spectral window. This arbitrary additional absorption also provides a consistent interpretation of the spectra of cloudy regions. Thus although the source of the absorption is unclear, it appears to characterize the opacity structure of Titan's atmosphere, independent of surface effects. We derive a surface albedo by including this additional source of opacity. The residuals between the calculated and measured spectra indicate an uncertainty in the surface albedo of ~0.02. At 5 μm the main source of opacity is Titan's haze. Titan's I/F at 4.8 μm, which is least affected by CO fluorescence, indicate a haze optical depth of 0.2, well within the uncertainties of the values estimated by DISR measurements.

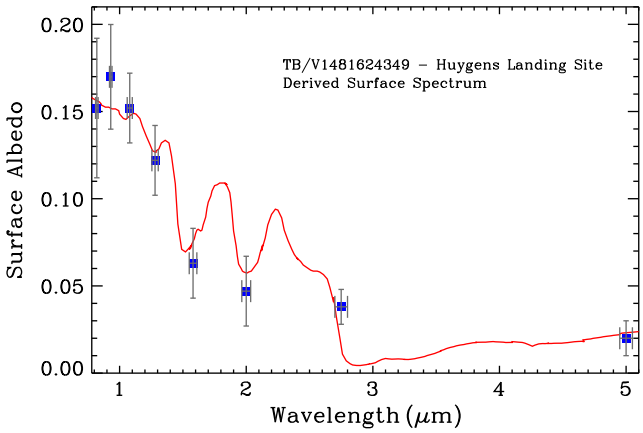

Fig. 11. Surface albedos derived from VIMS spectra of the probe landing site (blue squares) compared to a spectrum of Ganymede's leading hemisphere divided by 2 (red line).

This study indicates a need, particularly at 2 μm, for more theoretical and laboratory work on methane for the high pathlengths and low temperatures characteristic of Titan, similar to the recent work by (Kassi et al., 2008; Wang et al., 2010; Campargue et al., 2010; de Bergh et al., 2012), which have clarified and improved DISR derivations of the methane absorption.

The resulting surface spectrum of the Huygens landing site is relatively featureless, with the largest spectral modulation occurring between 1.58 μm and 1.28 μm (Fig. 11). This tendency is associated with the spectrum of water, as noted in prior ground-based spectra (Coustenis et al., 1995; Griffith et al., 2003). Water ice absorbs at 2.9 μm because of the ν_1 and ν_3 stretch bands, at 1.49 μm because of their first overtone combination, and at 1.9 μm because of the $\nu_2 + \nu_3$ combination band. The spectrum does not display a red color,[1] which is found in tholins and results from conjugated C–C and C=C bonds (Cruikshank et al., 1991). It is therefore not clear how organic sediments affect the derived surface albedo, with exception that they likely darken it. The derived spectrum from 0.8 to 5.0 μm is a slightly darker version of the disk-averaged surface albedo obtained from ground-based measurements (Griffith et al., 2003). Titan's surface albedos resemble those of Ganymede, which is somewhat unexpected, because while Ganymede is an icy jovian moon of similar size and density, it lacks a thick atmosphere, which on Titan ultimately produces organic surface sediments.

In general, the exposure of water ice would be somewhat surprising, because Titan's surface is continually accumulating photochemical byproducts of methane photolysis at a rate that would create a 0.6 km global layer over the course of its history (4.5 Gyr). Yet, VIMS observations reveal a range of different I/F values within the atmospheric windows, and therefore a range of surface

[1] For interpretation of color in Figs. 2–15, the reader is referred to the web version of this article.

compositions, (McCord et al., 2006; Barnes et al., 2007, 2009). In addition, Cassini images provide evidence of aeolian and fluvial erosion (Lorenz et al., 2006; Soderblom et al., 2007), arguing against a uniform blanket of photochemical sediments. Various Cassini measurements also indicate that the atmosphere was recently supplied (Tobie et al., 2005) and the surface recently eroded (Mousis and Schmitt, 2008), thereby suggesting that, at least in places, the water ice foundation of Titan's lithosphere may be exposed. This scenario is indicated by the analysis of VIMS data at 0.8–1.6 μm, which point to a water-rich surface surrounding Sinlap crater, suggesting the exposure of water ice through impact excavation (Soderblom et al., 2007). The Sinlap observations suggest that Titan consists of variable terrain of icy and organic components that depend on the moon's geology and weather. Potentially the landing site also exposes water ice through the erosion that formed its flood plain and the downward flowing drainage systems. The sample of eight albedos peered at though Titan's near-IR windows, are consistent with this scenario, but cannot establish it.

Acknowledgments

Research by C.A. Griffith, L. Doose, C. See, and M. Tomasko are funded by NASA's Planetary Astronomy and Cassini Data Analysis Programs. We thank Bruno Bézard and Pascal Rannou for their corrections and invaluable help with the manuscript. In addition, we benefitted from the suggestions by Christopher P. McKay and an anonymous reviewer.

Appendix A. Radiative transfer models

A.1. DISR doubling and adding analysis

The *in situ* Huygens DISR measurements were interpreted with a radiative transfer code, which was developed over many years. It uses the doubling and adding method for the scalar plane parallel approximation described by Hansen (1971) with several of the improvements suggested therein to speed the computation. Our scalar doubling and adding code begins by defining the single scattering properties within each layer at each wavelength, where the phase function can be specified in any required detail as a table of values between 0° and 180° scattering angles. The radiation field is divided into the singly-scattered component and the component that has been scattered more than once. We find the multiply-scattered component by layer doubling and adding, and then separately add the singly-scattered radiation field. We perform a Fourier analysis of the multiply-scattered component's azimuthal dependence, and double each Fourier component separately. Because most of the azimuthal dependence is in the singly-scattered radiation, we can use fewer Fourier orders than would otherwise be needed for the multiply-scattered radiation. We used 64 or fewer Fourier components for the multiply-scattered radiation.

We begin the layer doubling by finding the Scattering (S) and Transmission (T) functions of the multiply-scattered radiation field by analytically computing the first two orders of scattering for the homogeneous layers following Hovenier (1971). The optical depth at which the doubling starts is set to a value such that an error of less than 10^{-7} is caused by the omission of the multiple scattering terms. The S and T functions for the multiply-scattered radiation are computed by doubling S and T functions for thin layers until the required optical depth of each layer is reached. The singly-scattered radiation is added to the multiply-scattered radiation fields. The resulting S and T functions for the total radiation field are added upward and downward vertically in the atmosphere and saved for the atmosphere above and below each boundary. These functions permit the radiation field to be evaluated at each layer boundary. The resulting radiation fields may then be integrated over the fields of view and spectral bandpasses of the DISR instruments for comparison with the data.

For a defined zenith angle of the incident radiation, the radiance (intensity) is computed for many zenith angles of emergence and azimuth directions. The emergence angles are defined by the Gaussian quadrature approximation of $\int_0^1 I\mu d\mu$, where μ are the cosines of the zenith angles of the emergent rays. We used between 11 and 29 point Gaussian quadrature to define the solution. We use the "renormalization" technique of Hansen (1969) to insure conservation of energy even for the smallest number of zenith angles in the Gaussian quadrature.

The code supports up to 11 absorbing gases. Correlated-K methods may be applied to model the absorption where necessary. With respect to particulate scattering, subroutines include spherical particle Mie scattering, scattering by particles with Henyey-Greenstein phase functions, and scattering according to the empirical methods of Pollack and Cuzzi (1980). The code supports the surface scattering calculations described by Hapke's theory (Johnson et al., 1999). The atmosphere is defined by the scattering phase function, optical depth, and single scattering albedo of each of the 30 layers and the ground albedo. These values are published in Tomasko et al. (2008b,a).

We use the DISR doubling and adding code to model Cassini VIMS measurements of the probe landing site from 0.85 to 1.6 μm. We keep the same configuration that was used to analyze the Huygens DISR data. We divide the vertical structure of the atmosphere into 30 horizontally homogeneous layers. We assume an isotropically scattering (Lambertian) surface. In addition to absorption of methane, we include the effects of molecular scattering and scattering by fractal aggregates (Tomasko et al., 2008b). The DISR doubling and adding code along with documentation is available at the website http://doublingadding.webs.com/.

A.2. Discrete ordinates calculation

The discrete ordinates technique solves the radiative transfer equation by approximating the integral over vertical angles with a sum of discrete angular regions, or *streams*. The main difference in the assumptions underlying many discrete ordinates codes and the DISR doubling and adding code is the treatment of scattering phase function. The phase function of Titan's haze, derived from measurements recorded during Huygens descent, are published as a list of values at scattering angles that extend from forward scattering (0°) to backscattering (180°) (Tomasko et al., 2008b), and are handled as precise values in the DISR radiative transfer calculations. In contrast, in the discrete ordinates calculations, phase functions are usually specified from Legendre polynomials of the order of the number of streams. Generally this approximation is not problematical. However, DISR measurements determined that Titan's haze is highly forward peaked, so much so that at least 32 Legendre coefficients are needed to achieve a reasonable approximation of the forward peaked profiles at visible wavelengths. Penteado et al. (2010) approximate the forward peak of the DISR-derived phase functions with a less peaked Gaussian function that preserves the average probability of scattering for angles less than 20°. Here we derive the Legendre coefficients without approximating the forward peak.

The most commonly used discrete ordinates code is the publicly available DISORT, version 1.3, which is described in an extensive user manual (Stamnes et al., 1988). Adopting this software, we derive a new set of Legendre coefficients that fit the forward scattering peak of the phase function, with no approximation needed (Fig. 13). With less than 32 coefficients, the approximation to the phase functions at the shortest DISR wavelengths (which are most forward peaked), oscillate too highly about the actual value. To dampen this ringing, the DISR phase functions (Tomasko et al.,

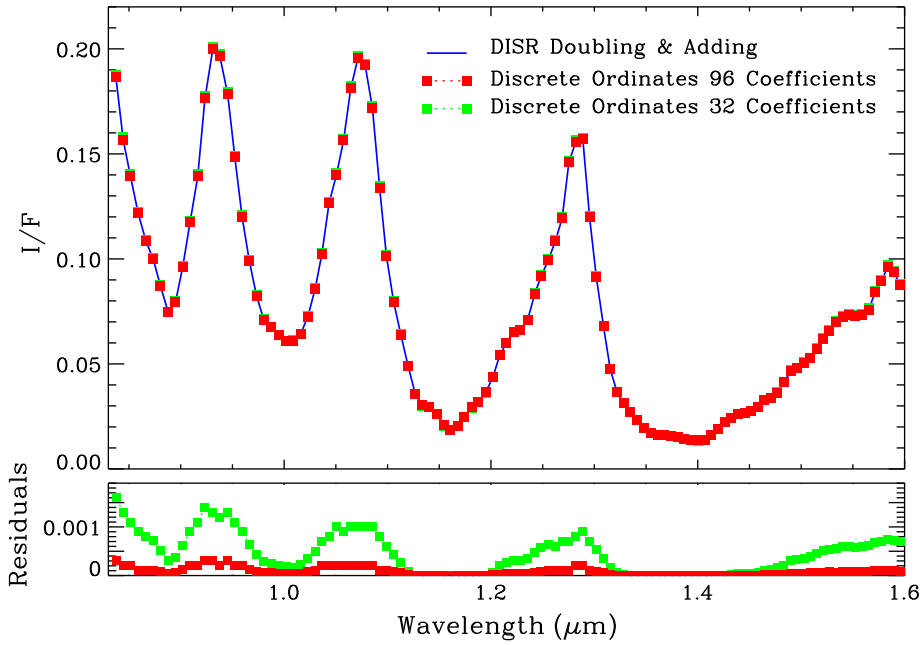

Fig. 12. Two calculations of Titan's spectrum, assuming incident and emergence angles of 36.721° and 36.844°, and an azimuth difference of 30°. The surface albedos adopted are those indicated by the solid line from Fig. 2. One spectrum was calculated with the DISORT2.0beta code and 96 Legendre coefficients, one with DISORT and 32 Legendre coefficients, Stamnes et al. (1988), the another from our DISR doubling and adding code. The spectra differ by at most 0.3%.

2008b) are mapped to 37 uniformly spaced phase angles. The 32 Legendre coefficients are then calculated, using a single value decomposition fit (from Numerical Recipes) to the phase function, with the first coefficient set to 1, as needed in the DISORT code. The resultant spectra match those calculated from the doubling and adding DISR code to within 0.85% (Fig. 12). The derived coefficients are not unique. Yet for the reader's convenience their values are given in Table 2 at several wavelengths that sample the range of values measured by DISR.

The benchmark calculations of these 32 coefficients (Appendix B) demonstrate a residual oscillation in the outgoing I/F with outgoing zenith angle. While this oscillation is largely smeared out in Titan's multiple scattering atmosphere (since the discrepancy is only 0.85%), it can be eliminated if we use the modified discrete ordinates version, DISORT2.0beta, which is set up to efficiently calculate scattering atmospheres that, like Titan's, require a large number of streams. This code accepts a large number of Legendre coefficients, and by using the intensity corrections developed by Nakajima and Tanaka (1988), reduces the computation to a small number of streams. We find that the DISR phase functions can be matched with 96 Legendre coefficients. The improved characterization of the DISR phase functions, as well as the duplication of the assumptions regarding Titan's atmospheric structure yields a discrete ordinates model (e.g. Fig. 12) that precisely replicates

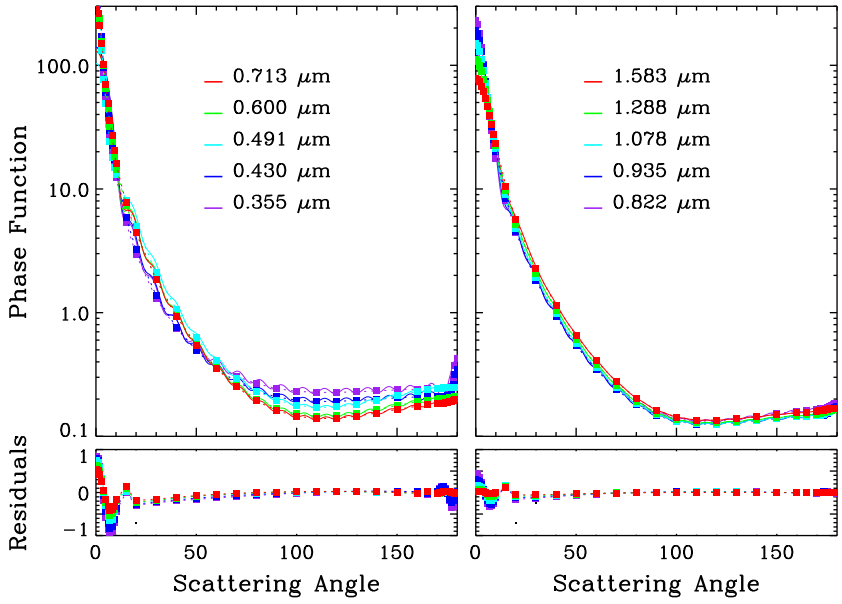

Fig. 13. The phase functions of the haze above 80 km as derived from the DISR measurements (squares) are compared to a 32 term Legendre polynomial fit (solid lines). The residuals as a fraction of the DISR measurements are shown below.

Table 2
Legendre coefficients for haze above 80 km.

0.355 μm	0.430 μm	0.491 μm	0.600 μm	0.713 μm	0.822 μm	0.935 μm	1.078 μm	1.288 μm	1.583 μm
1	1	1	1	1	1	1	1	1	1
0.7165	0.751	0.7396	0.7781	0.7872	0.7955	0.8044	0.8006	0.7926	0.7793
0.6472	0.6780	0.6393	0.6882	0.6964	0.7032	0.7099	0.7009	0.6856	0.6630
0.5778	0.6033	0.5275	0.5898	0.5996	0.6072	0.6143	0.6006	0.5786	0.5470
0.5236	0.5449	0.4484	0.5182	0.5280	0.5348	0.5406	0.5236	0.4966	0.4588
0.4778	0.4957	0.3830	0.4586	0.4688	0.4754	0.4805	0.4611	0.4307	0.3886
0.4381	0.4533	0.3322	0.4106	0.4205	0.4264	0.4303	0.4093	0.3766	0.3317
0.4027	0.4157	0.2917	0.3708	0.3799	0.3848	0.3873	0.3653	0.3311	0.2846
0.3711	0.3822	0.2595	0.3374	0.3455	0.3493	0.3501	0.3276	0.2927	0.2455
0.3421	0.3516	0.2335	0.3089	0.3157	0.3181	0.3172	0.2946	0.2595	0.2126
0.3157	0.3238	0.2123	0.2841	0.2895	0.2907	0.2881	0.2657	0.2309	0.1848
0.2908	0.2978	0.1945	0.2620	0.2660	0.2659	0.2617	0.2397	0.2057	0.1609
0.2678	0.2737	0.1793	0.2420	0.2447	0.2433	0.2377	0.2164	0.1834	0.1404
0.2458	0.2508	0.1658	0.2235	0.2249	0.2224	0.2155	0.1950	0.1633	0.1223
0.2252	0.2293	0.1536	0.2061	0.2063	0.2030	0.1949	0.1754	0.1451	0.1064
0.2052	0.2086	0.1421	0.1895	0.1887	0.1845	0.1756	0.1570	0.1284	0.09210
0.1864	0.1890	0.1311	0.1735	0.1718	0.1671	0.1574	0.1399	0.1130	0.07923
0.1680	0.1701	0.1205	0.1581	0.1556	0.1503	0.1402	0.1239	0.09873	0.06750
0.1508	0.1522	0.1101	0.1431	0.1400	0.1344	0.1240	0.1089	0.08555	0.05688
0.1340	0.1350	0.09985	0.1286	0.1250	0.1192	0.1087	0.09475	0.07333	0.04723
0.1185	0.1189	0.08977	0.1145	0.1107	0.1048	0.09440	0.08168	0.06217	0.03861
0.1034	0.1035	0.07993	0.1010	0.09696	0.09116	0.08104	0.06956	0.05199	0.03095
0.08972	0.08940	0.07031	0.08797	0.08395	0.07836	0.06875	0.05852	0.04288	0.02431
0.07660	0.07602	0.06103	0.07560	0.07167	0.06640	0.05746	0.04848	0.03478	0.01865
0.06487	0.06397	0.05207	0.06387	0.06018	0.05536	0.04727	0.03952	0.02774	0.01397
0.05375	0.05268	0.04358	0.05290	0.04952	0.04522	0.03809	0.03157	0.02167	0.01021
0.04404	0.04275	0.03550	0.04265	0.03970	0.03603	0.02998	0.02463	0.01656	0.007280
0.03487	0.03353	0.02803	0.03328	0.03080	0.02777	0.02284	0.01862	0.01228	0.005065
0.02707	0.02562	0.02106	0.02472	0.02278	0.02044	0.01666	0.01348	0.008753	0.003429
0.01971	0.01835	0.01492	0.01726	0.01581	0.01410	0.01138	0.009154	0.005879	0.002232
0.01367	0.01236	0.009428	0.01076	0.009811	0.008715	0.007001	0.005585	0.003554	0.001334
0.008067	0.007038	0.005125	0.005724	0.005174	0.004553	0.003616	0.002863	0.001809	0.0006804
0.004024	0.003271	0.001889	0.002056	0.001841	0.001609	0.001275	0.0009847	0.0006095	0.0002291

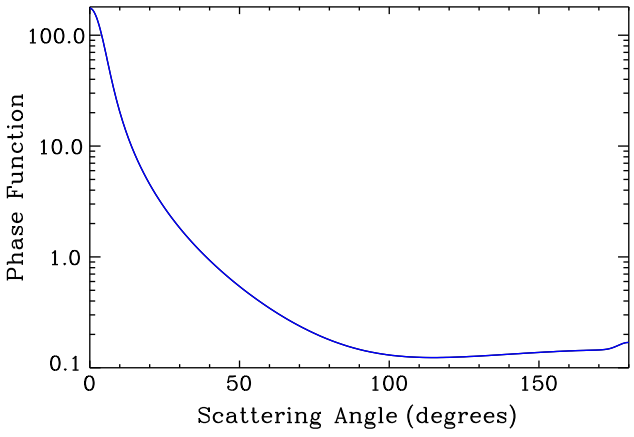

Fig. 14. The phase function used in the three test cases.

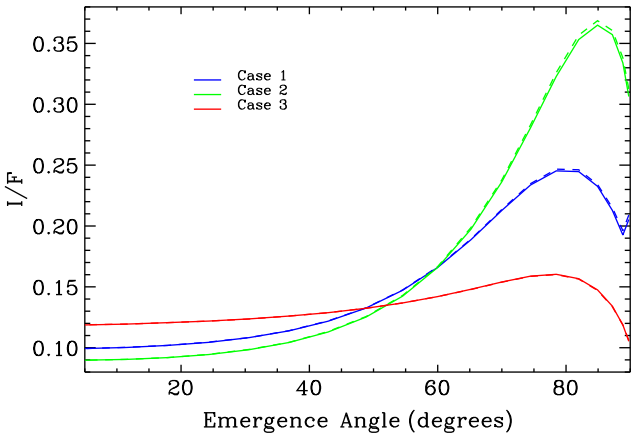

Fig. 15. The outgoing I/F as a function of the outgoing angle, θ_s.

the results of the DISR doubling and adding model, while significantly reducing the calculation time.

The discrete ordinates calculations of Titan presented here involve 70 layers, that extend from 375 km down to the surface. The lower 15 km of the atmosphere is sampled finely (with 15 layers) so as to better define the variable methane absorption. All DISR-derived haze and methane parameters are interpolated to the vertical grid of our model. We adopt the wavelength grid of the DISR measurements when using their derived opacity structure, and a grid spacing of 0.05 cm^{-1} for longer wavelengths that include line-by-line calculations.

Table 3
Parameters of test models.

	Case 1	Case 2	Case 3
θ	36.721	45.0	20.0
$\Delta\phi$ Angle	30.0	10.0	150.0
Layers	2	2	1
τ_1/τ_1	0.5/0.5	0.25/0.75	1.0
ω_1/ω_2	0.96/0.96	0.96/0.96	0.98

Appendix B. Comparison models

Here we present three benchmark calculations that can be used to compare radiative transfer calculations with that derived from the *in situ* Huygens Probe DISR measurements, to determine

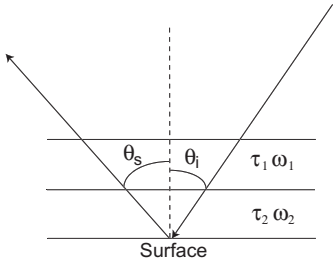

Fig. 16. The geometry of the two layer models for the doubling and adding and DIRSORT calculations.

whether the phase function is handled correctly, and whether, over all, the calculation is correct.

Each calculation assumes a Lambertian surface with a ground albedo of 0.1, as well as the phase function detailed in Fig. 14. Since these test radiative transfer calculations do not involve thermal radiation, they are independent of wavelength. The remaining parameters, including the optical depths (τ), single scattering albedo (ω), incident angle (θ) and the difference between the incident and scattering azimuthal angles ($\Delta\phi$) that specify these 1–2 layer models are given in Table 3.

The radiative transfer program calculates the top of the atmosphere outgoing I/F as a function of the outgoing angles θ_s (Fig. 15). The geometry of the models are shown in Fig 16. The ascii files for the input variables and resultant I/F values are provided by at the website (http://doublingadding.webs.com/) under "Test Cases".

References

Barnes, J.W. et al., 2009. VIMS spectral mapping observations of Titan during the Cassini prime mission. Planet. Space Sci. 57, 1950–1962.

Barnes, J.W., Brown, R.H., Soderblom, L., Buratti, B.J., Sotin, C., Rodriguez, S., Le Mouèlic, S., Baines, K.H., Clark, R., Nicholson, P., 2007. Global-scale surface spectral variations on Titan seen from Cassini/VIMS. Icarus 186, 242–258.

Cabane, M., Chassefiere, E., Israel, G., 1992. Formation and growth of photochemical aerosols in Titan's atmosphere. Icarus 96, 176–189.

Campargue, A., Wang, L., Liu, A.W., Hu, S.M., Kassi, S., 2010. Empirical line parameters of methane in the 1.63–1.48 μm transparency window by high sensitivity Cavity Ring Down Spectroscopy. Chem. Phys. 373, 203–210.

Courtin, R., Gautier, D., McKay, C.P., 1995. Titan's thermal emission spectrum: Reanalysis of the Voyager infrared measurements. Icarus 114, 144–162.

Coustenis, A., Lellouch, E., Maillard, J.P., McKay, C.P., 1995. Titan's surface: composition and variability from the near-infrared albedo. Icarus 118, 87–104.

Coustenis, A., Negrão, A., Salama, A., Schulz, B., Lellouch, E., Rannou, P., Drossart, P., Encrenaz, T., Schmitt, B., Boudon, V., Nikitin, A., 2006. Titan's 3-micron spectral region from ISO high-resolution spectroscopy. Icarus 180, 176–185.

Cruikshank, D.P., Allamandola, L.J., Hartmann, W.K., Tholen, D.J., Brown, R.H., Matthews, C.N., Bell, J.F., 1991. Solid C triple bond N bearing material on outer Solar System bodies. Icarus 94, 345–353.

de Bergh, C. et al., 2012. Applications of a new set of methane line parameters to the modeling of Titan's spectrum in the 1.58 micron window. Planet. Space Sci. 61, 85–98.

Flasar, F.M., Samuelson, R.E., Conrath, B.J., 1981. Titan's atmosphere – Temperature and dynamics. Nature 292, 693–698.

Griffith, C.A. et al., 2009. Characterization of clouds in Titan's tropical atmosphere. Astrophys. J. 702, L105–L109.

Griffith, C.A., Owen, T., Wagener, R., 1991. Titan's surface and troposphere, investigated with ground-based, near-infrared observations. Icarus 93, 362–378.

Griffith, C.A., Owen, T., Geballe, T.R., Rayner, J., Rannou, P., 2003. Evidence for the exposure of water ice on Titan's surface. Science 300, 628–630.

Hansen, J.E., 1969. Radiative transfer by doubling very thin layers. Astrophys. J. 155, 565–573.

Hansen, J.E., 1971. Multiple scattering of polarized light in planetary atmospheres. Part I. The doubling method. J. Atmos. Sci. 28, 120–125.

Hovenier, J.W., 1971. Multiple scattering of polarized light in planetary atmospheres. Astron. Astrophys. 13, 7–29.

Israel, G., Chassefiere, E., Cabane, M., Raulin, F., Boon, J.J., 1991. Aerosols in Titan's atmosphere – Models, sampling techniques and chemical analysis. Ann. Geophys. 9, 1–13.

Johnson, T.J., Wilson, C.R., Chao, B.F., 1999. Oceanic angular momentum variability estimated from the Parallel Ocean Climate Model, 1988–1998. J. Geophys. Res. 104, 25183–25196.

Karkoschka, E., Tomasko, M.G., 2010. Methane absorption coefficients for the jovian planets from laboratory, Huygens, and HST data. Icarus 205, 674–694.

Kassi, S., Gao, B., Romanini, D., Campargue, A., 2008. The near-infrared (1.30–1.70 μm) absorption spectrum of methane down to 77 K. Phys. Chem. Chem. Phys. (Incorp. Faraday Trans.) 10, 4410–4419.

Keller, H.U., Grieger, B., Küppers, M., Schröder, S.E., Skorov, Y.V., Tomasko, M.G., 2008. The properties of Titan's surface at the Huygens landing site from DISR observations. Planet. Space Sci. 56, 728–752.

Khare, B.N., Sagan, C., Arakawa, E.T., Suits, F., Callcott, T.A., Williams, M.W., 1984. Optical constants of organic tholins produced in a simulated Titanian atmosphere – From soft X-ray to microwave frequencies. Icarus 60, 127–137.

Khare, B.N., Sagan, C., Thompson, W.R., Arakawa, E.T., Meisse, C., Tuminello, P.S., 1994. Optical properties of poly-HCN and their astronomical applications. Can. J. Chem. 72, 678–694.

Lavvas, P., Griffith, C.A., Yelle, R.V., 2011. Condensation in Titan's atmosphere at the Huygens landing site. Icarus 215, 732–750.

Lellouch, E., Coustenis, A., Gautier, D., Raulin, F., Dubouloz, N., Frere, C., 1989. Titan's atmosphere and hypothesized ocean – A reanalysis of the Voyager 1 radio-occultation and IRIS 7.7-micron data. Icarus 79, 328–349.

Lellouch, E., Coustenis, A., Sebag, B., Cuby, J., López-Valverde, M., Schmitt, B., Fouchet, T., Crovisier, J., 2003. Titan's 5-μm window: Observations with the Very Large Telescope. Icarus 162, 125–142.

Lindal, G.F., Wood, G.E., Hotz, H.B., Sweetnam, D.N., Eshleman, V.R., Tyler, G.L., 1983. The atmosphere of Titan – An analysis of the Voyager 1 radio occultation measurements. Icarus 53, 348–363.

Lorenz, R.D. et al., 2006. The sand seas of Titan: Cassini RADAR observations of longitudinal dunes. Science 312, 724–727.

McCord, T.B. et al., 2006. Composition of Titan's surface from Cassini VIMS. Planet. Space Sci. 54, 1524–1539.

McKay, C.P. et al., 2001. Physical properties of the organic aerosols and clouds on Titan. Planet. Space Sci. 49, 79–99.

McKay, C.P., Pollack, J.B., Courtin, R., 1989. The thermal structure of Titan's atmosphere. Icarus 80, 23–53.

McKay, C.P., Martin, S.C., Griffith, C.A., Keller, R.M., 1997. Temperature lapse rate and methane in Titan's troposphere. Icarus 129, 498–505.

McKellar, A.R.W., 1989. Low-temperature infrared absorption of gaseous N_2 and $N_2 + H_2$ in the 2.0–2.5 micron region – Application to the atmospheres of Titan and Triton. Icarus 80, 361–369.

Mousis, O., Schmitt, B., 2008. Sequestration of ethane in the cryovolcanic subsurface of Titan. Astrophys. J. 677, L67–L70.

Nakajima, T., Tanaka, M., 1988. Algorithms for radiative intensity calculations in moderately thick atmospheres using a truncation approximation. J. Quant. Spectrosc. Radiat. Transf. 40, 51–69.

Niemann, H.B. et al., 2005. The abundances of constituents of Titan's atmosphere from the GCMS instrument on the Huygens Probe. Nature 438, 779–784.

Niemann, H.B. et al., 2010. Composition of Titan's lower atmosphere and simple surface volatiles as measured by the Cassini–Huygens Probe gas chromatograph mass spectrometer experiment. J. Geophys. Res. (Planets) 115, 1–22.

Penteado, P.F., Griffith, C.A., 2010. Ground-based measurements of the methane distribution on Titan. Icarus 206, 345–351.

Penteado, P.F., Griffith, C.A., Tomasko, M.G., Engel, S., See, C., Doose, L., Baines, K.H., Brown, R.H., Buratti, B.J., Clark, R., Nicholson, P., Sotin, C., 2010. Latitudinal variations in Titan's methane and haze from Cassini VIMS observations. Icarus 206, 352–365.

Pollack, J.B., Cuzzi, J.N., 1980. Scattering by nonspherical particles of size comparable to wavelength – A new semi-empirical theory and its application to tropospheric aerosols. J. Atmos. Sci. 37, 868–881.

Rages, K., Pollack, J.B., 1983. Vertical distribution of scattering hazes in Titan's upper atmosphere. Icarus 55, 50–62.

Rannou, P., McKay, C.P., Lorenz, R.D., 2003. A model of Titan's haze of fractal aerosols constrained by multiple observations. Planet. Space Sci. 51, 963–976.

Rannou, P., Cours, T., Le Mouélic, S., Rodriguez, S., Sotin, C., Drossart, P., Brown, R., 2010. Titan haze distribution and optical properties retrieved from recent observations. Icarus 208, 850–867.

Rothman, L.S. et al., 2009. The HITRAN 2008 molecular spectroscopic database. Journal of Quantitative Spectroscopy and Radiative Transfer 110, 533–572.

Samuelson, R.E., Nath, N.R., Borysow, A., 1997. Gaseous abundances and methane supersaturation in Titan's troposphere. Planet. Space Sci. 45, 959–980.

Schröder, S.E., Keller, H.U., 2009. The unusual phase curve of Titan's surface observed by Huygens' Descent Imager/Spectral Radiometer. Planet. Space Sci. 57, 1963–1974.

Soderblom, L.A. et al., 2007. Correlations between Cassini VIMS spectra and RADAR SAR images: Implications for Titan's surface composition and the character of the Huygens Probe landing site. Planet. Space Sci. 55, 2025–2036.

Stamnes, K., Tsay, S.-C., Jayaweera, K., Wiscombe, W., 1988. Numerically stable algorithm for discrete-ordinate-method radiative transfer in multiple scattering and emitting layered media. Appl. Opt. 27, 2502–2509.

Tobie, G., Grasset, O., Lunine, J.I., Mocquet, A., Sotin, C., 2005. Titan's internal structure inferred from a coupled thermal–orbital model. Icarus 175, 496–502.

Tomasko, M.G. et al., 1997. Models of the penetration of sunlight into the atmosphere of Titan. ESA SP-1177 1177, 345–358.

Tomasko, M.G. et al., 2005. Rain, winds and haze during the Huygens Probe's descent to Titan's surface. Nature 438, 765–778.

Tomasko, M.G. et al., 2008b. A model of Titan's aerosols based on measurements made inside the atmosphere. Planet. Space Sci. 56, 669–707.

Tomasko, M.G., Bézard, B., Doose, L., Engel, S., Karkoschka, E., 2008a. Measurements of methane absorption by the descent imager/spectral radiometer (DISR) during its descent through Titan's atmosphere. Planet. Space Sci. 56, 624–647.

Wang, L., Kassi, S., Campargue, A., 2010. Temperature dependence of the absorption spectrum of CH4 by high resolution spectroscopy at 81K: (I) The region of the $2v3$ band at 1.66μm. J. Quant. Spectrosc. Radiat. Transf. 111, 1130–1140.

West, R.A., Smith, P.H., 1991. Evidence for aggregate particles in the atmospheres of Titan and Jupiter. Icarus 90, 330–333.

Young, E.F., Rannou, P., McKay, C.P., Griffith, C.A., Noll, K., 2002. A three-dimensional map of Titan's tropospheric haze distribution based on Hubble Space Telescope Imaging. Astron. J. 123, 3473–3486.